PHYSICAL REVIEW B VOLUME 23, NUMBER 12 15 JUNE 1981

Determination of the threshold-energy surface for copper using *in-situ* electrical-resistivity measurements in the high-voltage electron microscope

Wayne E. King
Department of Materials Science and Engineering, Northwestern University, Evanston, Illinois 60201

K. L. Merkle
Materials Science Division, Argonne National Laboratory, Argonne, Illinois 60439

M. Meshii
Department of Materials Science and Engineering, Northwestern University, Evanston, Illinois 60201

(Received 14 August 1980)

A detailed study of the anisotropy of the threshold energy for Frenkel-pair production in copper was carried out experimentally, using *in-situ* electrical-resistivity measurements in the high-voltage electron microscope. These electrical-resistivity measurements, which are sensitive to small changes in point-defect concentration, were used to determine the damage or defect production rate. Damage-rate measurements in copper single crystals were carried out for ~40 incident electron-beam directions and six electron energies from 0.4 to 1.1 MeV. The total cross section for Frenkel-pair production is proportional to the measured damage rate and can be theoretically calculated if the form of the threshold-energy surface is known. Trial threshold-energy surfaces were systematically altered until a "best fit" of the calculated to the measured total cross sections for Frenkel-pair production was obtained. The average threshold energy of this surface is 28.5 eV. The minimum threshold energy is 18 ± 2 eV and is located near $\langle 100 \rangle$. A ring of very high threshold energy (> 50 eV) surrounds the $\langle 111 \rangle$ direction. A damage function for single-defect production was derived from this surface and was applied to defect-production calculations at higher recoil energies. This function rises rather sharply from a value of zero at 17 eV to 0.8 at 42 eV. It has the value of 0.5 at 24.5 eV. Above 30 eV the slope of the curve begins to decrease, reflecting the presence of the high-energy regions of the threshold-energy surface. Both topographical and quantitative comparisons of the present surface with those in the literature were presented. Based on a χ^2 goodness-of-fit test, the present surface was found to predict the experimentally observed total cross sections for Frenkel-pair production significantly better than the other available surfaces. Also, the goodness of fit varied substantially less with energy and direction for the present surface.

I. INTRODUCTION

It is of great interest, both in the applied and basic sciences, to be able to quantitatively predict the damage state produced in a material by irradiation with energetic particles. In the low-temperature case, where the irradiation-induced defect structure is preserved, studies of defect production involve the experimental determination of the damage function, $\nu(T)$, which gives the average number of point defects (Frenkel pairs) that are formed as a function of transferred (recoil) energy T for an isotropic distribution of recoil directions. The low-energy portion of the damage function, $\nu(T) \leq 1$, which is simply the probability of forming a stable Frenkel pair for a collision in a random direction, may be investigated by a detailed study of the anisotropy of the threshold energy for Frenkel-pair production. The results of such an investigation are vitally important as a basis for theoretically predicting the damage produced at higher recoil energies. The basic question that needs to be answered is this: For a projectile of energy E_1 incident on a given target, on the average, how many defects will be formed as a result of the interaction of the projectile with the target? This quantity is proportional to the total-displacement cross section, which can be calculated by

$$\sigma_d(E_1) = \int_0^{T_m} \nu(T) \frac{d\sigma(T;E_1)}{dT}\, dT \tag{1}$$

for an isotropic distribution of recoil directions, where $\sigma_d(E_1)$ is the total-displacement cross section, $\nu(T)$ is the damage function, $d\sigma(T;E_1)/dT$ is the differential recoil-energy cross section or the probability of producing a recoil of energy between T and $T+dT$ due to the impact of the projectile of energy E_1 with the target atom, and T_m is the maximum energy transferred to the target atom in a head-on collision. The spatial average of the directionally dependent damage function is given by

$$\nu(T) = \langle \nu(\Theta_2, \Phi_2; T) \rangle_{(\Theta_2, \Phi_2)}, \tag{2}$$

where Θ_2 and Φ_2 are polar and azimuthal angles, respectively, measured with respect to the [001] pole. The latter reflects the anisotropy of the threshold energy for Frenkel-pair production which can be represented by a threshold-energy surface. Once the threshold-energy surface has been established, the damage function for $\nu(T) \leq 1$ follows directly from Eq. (2). In addition to the

damage function, a detailed threshold-energy surface may give insight into the basic mechanisms of atomic displacement and reflect the magnitude of interatomic forces at separations smaller than the nearest-neighbor distance.

The experimental technique that was employed in the present work to determine the anisotropy of the threshold energy for Frenkel-pair production in copper was *in-situ* electrical-resistivity measurements below 10 K in the high-voltage electron microscope (HVEM). In the past, both electrical resistivity and high-voltage electron microscopy have been used separately to study the anisotropy of the threshold energy for Frenkel-pair production, with electrical-resistivity measurements concentrating on small changes in the density of isolated Frenkel pairs at low temperature, and HVEM studies concentrating on the observation of measurable changes in visible defect clusters formed primarily at elevated temperatures (see reviews in Refs. 1–4). The present *in-situ* study takes advantage of the high-energy electron beams produced by the HVEM, which are orders of magnitude more intense and less divergent than beams of typical electron accelerators. In addition, the HVEM provides for precise specimen alignment and electron dosimetry. Coupled with the electrical-resistivity measurements, which give a direct indication of small changes in the defect concentration, *in-situ* irradiation provides a unique tool to investigate the anisotropy of the threshold energy for Frenkel-pair production.

In the present work, *in-situ* damage-rate measurements on thin, single-crystal copper films were carried out for electron irradiations in 40 crystallographic directions at six energies ranging from 0.4 to 1.1 MeV. The measured total cross sections for Frenkel-pair production were compared to the total cross sections calculated from trial threshold-energy surfaces composed of 41 ($5°\times 5°$) blocks distributed over the unit triangle of a cubic crystal (defined by the directions ⟨100⟩, ⟨110⟩, and ⟨111⟩). A derivative-type, unconstrained-optimization scheme[5] was used to find the best-fit threshold-energy surface consistent with the present data. The results were used to derive a damage function for $\nu(T)<1$.

II. BASIC PRINCIPLES

The coordinate system that will be used when referring to the incident electron-beam direction and the target-atom recoil angles and directions is the cubic [001] standard stereographic projection shown in Fig. 1. The upper-case Greek letters (Θ,Φ) refer to angles measured with respect to the [001] pole while the lower-case Greek letters (θ,ϕ) refer to angles measured with respect to the incident-beam direction. The subscript 1 refers to the incident electrons and the subscript 2 refers to the target atom. The direction of the incident electron beam is specified by the polar angle Θ_1 and azimuthal angle Φ_1. The incident electrons are scattered by angles (θ_1,ϕ_1) (not shown). As a result of this scattering event, the target atom recoils at angles (θ_2,ϕ_2) in the crystal directions specified by polar angle Θ_2 and azimuthal angle Φ_2. The angle ϕ_2 is the included angle defined by the intersection of the two great circles containing the poles $(\pi/2,\Phi_1)$, (Θ_1,Φ_1) and (Θ_1,Φ_1), (Θ_2,Φ_2).

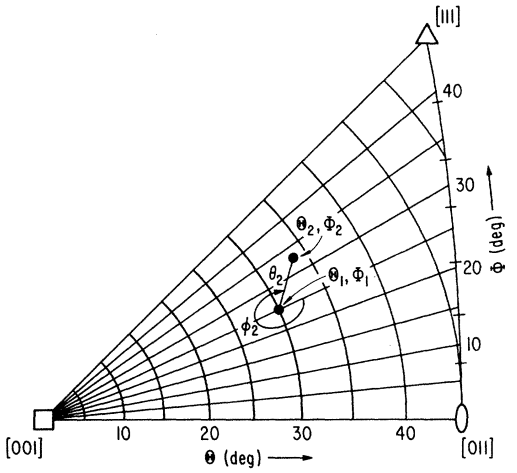

FIG. 1. The coordinate system, showing the electron-beam direction (Θ_1,Φ_1), recoil angle (θ_2,ϕ_2), and the recoil direction (Θ_2,Φ_2).

The probability for a recoil to create a stable Frenkel pair is a function of both the recoil direction and the transferred energy T and is assumed to be a step function going from a probability of zero to one when the transferred energy equals or exceeds the threshold energy in the recoil direction;

$$\nu(\Theta_2,\Phi_2;T)=\begin{cases}0 \text{ for } T<T_d(\Theta_2,\Phi_2)\\ 1 \text{ for } T\geq T_d(\Theta_2,\Phi_2)\end{cases}. \tag{3}$$

For a homogeneous, parallel beam of monoenergetic electrons of energy E_1 the total cross section for Frenkel-pair production, $\sigma_d(\Theta_1,\Phi_1;E_1)$, is given by

$$\sigma_d(\Theta_1,\Phi_1;E_1)=\int_0^{2\pi}\int_0^{\pi/2}\frac{d\sigma(\theta_2;E_1)}{d\theta_2}\frac{d\phi_2}{2\pi}\nu(\Theta_2,\Phi_2;T)d\theta_2\,, \tag{4}$$

where $d\sigma(\theta_2;E_1)/d\theta_2$ is the differential cross section, which can be related to the differential scattering cross section $d\sigma(\theta_1;E_1)/d\theta_1$. Since the scattering angle in the laboratory frame of reference

θ_1 is, for the electron case, nearly equal to the scattering angle in both the relative and the center-of-mass frames of reference, we have the relation

$$\theta_2 = \tfrac{1}{2}(\pi - \theta_1) . \quad (5)$$

The differential recoil cross section weights the distribution of recoil directions to directions away from the incident-beam direction, that is, toward increasing θ_2. This implies that, in general, most of the stable Frenkel pairs result from recoils in directions other than the incident electron-beam direction. Consequently, any measured total cross section for Frenkel-pair production contains contributions from many directions and so does not provide direct information on the anisotropy of the threshold energy for Frenkel-pair production. The situation would be further complicated if multiple scattering were included in Eq. (4). We assume that in the case of thin specimens, multiple scattering may be neglected.[6]

III. EXPERIMENTAL METHOD

A. The specimen stage

A side-entry type, single-tilt, cryogenic specimen stage was designed and developed for use in the Kratos-AEI EM7 1200-keV HVEM at Argonne National Laboratory. With this stage, electrical-resistivity measurements as well as irradiation and observation of the same specimen were possible *in situ*. The specimen stage was designed as a flow cryostat that used helium gas or liquid as a coolant to attain and maintain any temperature in the range <10 to 300 K. The helium flow cooled both a copper specimen block, which supported the specimen, and its concentric cold shield, which reduced conductive and radiative heat flow to the specimen block and the contamination rate at the specimen. The specimen was mounted on a polished sapphire specimen holder so that the portion to be irradiated lay across a small hole, and the holder was pressed into the specimen block using an indium gasket. The path of the electron beam from the accelerator to the specimen was thus unobstructed, which ensured the minimum beam divergence that could be obtained using the electron optics of the HVEM. A platinum resistance thermometer was fastened directly to the copper specimen block.

B. Procedure

1. Specimen preparation

Thin (~0.4-μm) single-crystal films from <0.001% metallic impurities Alpha copper were deposited on ⟨100⟩-cleaved sodium chloride substrates in a vacuum of 1.3×10^{-5} Pa using the resistance-heating method. The ⟨100⟩ epitaxy was obtained by heating the substrate to 300-350 °C. The sodium chloride substrate was cleaved into 3×3 mm^2 squares and the metal film was floated off in water when the sodium chloride dissolved. It was picked up on a thin collodion film that was stretched tightly across a brass ring. The collodion film, with the specimen attached, was lowered onto a 3-mm-diam sapphire disk prepared with gold contact pads and a 1-mm-diam central hole. The collodion film and specimen were then stretched taut to obtain the optimum specimen flatness. The collodion film was partially dissolved in an acetone vapor, after which it was completely dissolved in a condensation washer using amyl acetate as a solvent. The disk, with the specimen adhering tightly, was mounted in an ion-milling mask holder and the specimen was then ion milled using 2-keV argon ions to obtain the configuration shown in Fig. 2. Following the ion milling, gold wires were welded to the gold contact pads on the sapphire disk. The specimen was then mounted in the specimen stage and the final electrical connections were made. All the electrical-resistivity measurements were carried out *in situ* in the HVEM with the objective lens deenergized. The geometry factor was determined from the measurement of the room-temperature resistance of the specimen. The specimen was then cooled to <10 K, where the sensitivity of the electrical-resistivity measurement was verified to be better than 1×10^{-11} Ω cm.

2. Irradiation

The specimens were aligned using Kikuchi patterns such that the major crystallographic direction [001], which was perpendicular to the specimen surface, was nearly parallel to the electron beam. This electron-beam direction was called the reference direction. After each irradiation

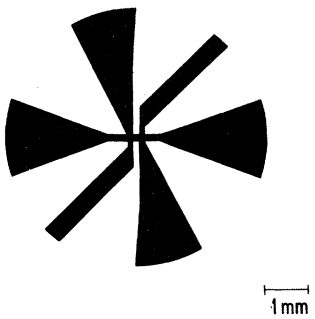

FIG. 2. Specimen configuration used for *in-situ* electrical resistivity measurements in high-voltage electron microscope.

step, measurement of the change $d\Delta\rho$ in the specimen electrical resistivity due to the dose increment $d\phi$, yielded the damage rate $d\Delta\rho/d\phi$. The specimen was then tilted by an angular increment that was typically a multiple of 5°, and another damage-rate measurement was carried out. Finally, the specimen was returned to the reference direction for a third damage-rate measurement. This procedure was carried out cyclically, increasing the tilt angle with each cycle, until the tilt limit (~47°) was reached. After the procedure was completed, it was repeated at five additional energies and a Kikuchi map of the tilt path was photographically recorded, with additional Kikuchi patterns recorded at the tilt angles that were used for irradiation. The entire procedure was performed for four different tilt paths, three on one specimen and one on another. The electron dose could be measured accurately to within 5%. The electron energy is known to an accuracy of 1%. The electron-beam heating was less than 2 K during irradiation.

IV. THEORETICAL ANALYSIS

A. Derivation of a threshold-energy surface

The aim of this work was to determine a directionally dependent damage function, $\nu(\Theta_2,\Phi_2;T)$, and thus a threshold-energy surface, $T_d(\Theta_1,\Phi_2)$, from Eq. (4) based on the observed total cross sections for Frenkel-pair production, $\sigma_d^{\rm obs}(\Theta_1,\Phi_1;E_1)$. Since it is impossible to analytically unfold Eq. (4) and directly extract the threshold-energy surface, an alternative approach was taken: Given a trial threshold-energy surface, values for the total cross section for Frenkel-pair production $\sigma_d^{\rm calc}(\Theta_1,\Phi_1;E_1)$ were calculated for directions and energies corresponding to $\sigma_d^{\rm obs}(\Theta_1,\Phi_1;E_1)$.

For the calculations of the total cross section for Frenkel-pair production, it was necessary to know the law governing the interaction of the electrons and the atomic nuclei of the solid, that is, the elastic nuclear scattering commonly referred to as the differential scattering cross section, $d\sigma(\Theta_1;E_1)/d\Theta_1$. Oen's tables,[7] which give the ratio of Mott to Rutherford differential scattering cross sections, were used to obtain the differential cross section $d\sigma(\Theta_2;E_1)/d\Theta_2$. A computer code was then employed to perform the double integration of Eq. (4) for any arbitrary anisotropic threshold-energy surface composed of ~41 discrete 5°×5° blocks distributed over the unit triangle in the cubic system. Integration steps of two degrees in the azimuthal recoil angle ϕ_2 and one degree in the polar recoil angle θ_2 were used. The accuracy of these calculated total cross sections for Frenkel-pair production was ~4%, when compared with those given in Oen's tables[7] for an isotropic threshold-energy surface.

The derivation of a threshold-energy surface, based upon measured total cross sections for Frenkel-pair production, began by assigning "first-guess" values to the 41 (5°×5°) regions of the unit triangle and then calculating the cross sections corresponding to beam directions used in the experiment. These calculated cross sections were compared with the measured cross sections using the χ^2 goodness-of-fit test. The χ^2 statistic was defined as

$$\chi^2=\frac{1}{k-s}\sum_{i=1}^{k}\left(\frac{\sigma_i^{\rm obs}-\sigma_i^{\rm calc}}{W_i}\right)^2, \tag{6}$$

where $\sigma_i^{\rm obs}$ and $\sigma_i^{\rm calc}$ correspond to the observed and calculated total cross sections for Frenkel-pair production, k is the number of observations, s is the number of independently adjustable 5°×5° threshold-energy regions, $k-s$ is the number of degrees of freedom, and W_i is the absolute error associated with each observed total cross section for Frenkel-pair production. A derivative-type unconstrained-optimization scheme[5] was used to find the best-fit threshold-energy surface, i.e., χ^2 close to one, consistent with the present 0.502, 0.600, 0.701, 0.910, and 1.106-MeV data. In order to avoid possible uncertainties in the results due to electron channeling in thin films as proposed by Bauer, Anderman, and Sosin,[8] the total cross sections for Frenkel-pair production from directions that were close to the low-index poles were deleted from the analysis. The "first-guess" threshold-energy surface used in the analysis was based on the surfaces of Jung *et al.*[9] and Schwartz *et al.*[10]

B. Assumptions

The following assumptions and approximations were made to facilitate the analysis of the data: (1) The probability of forming a stable Frenkel pair increases from zero to one at the threshold energy for a particular direction (Θ_2,Φ_2), and remains at one for all energies used in the analysis. (2) The electron beam is a homogeneous parallel beam of monoenergetic particles, that is, energy loss and multiple scattering are negligible.[11] (3) Changes in the electrical resistivity of copper are proportional to the changes in the defect concentration and are independent of defect configuration.[12,13] (4) The correction for the electrical-resistivity size effect is independent of defect configuration[8] and can be made using the Fuchs-Sondheimer theory.[14] (5) Subthreshold defect production is negligible. (6) The effects of dynamic electron diffraction on the damage rate are negligible.[15-20]

V. RESULTS

A. Experimental observations

The measured damage rates were corrected for the electrical-resistivity size effect using the Fuchs-Sondheimer theory.[14] The probability of specular reflection of the conduction electrons at the specimen surface was taken to be zero and the ratio of the film thickness of the mean free path of the conduction electrons was chosen in a self-consistent manner: Damage rates for particular incident electron-beam directions were first normalized to damage rates in the reference direction at the same value of irradiation-induced electrical resistivity; normalized damage rates calculated from these uncorrected rates are independent of the size effect. Damage rates adjusted by a size-effect parameter, corrected for the saturation effect (see Fig. 3), and normalized to the reference direction damage rate, were then fit to the normalized damage rates from the uncorrected data by varying the size-effect parameter until a best fit was found. Data from each tilt path and energy were independently corrected. This technique provided an optimum selection of the size-effect parameter.

The saturation-effect correction was necessary because the total cross sections for Frenkel-pair production, as calculated from Eq. (4), refer to defect production in an undisturbed lattice. Damage rates for an undisturbed lattice, i.e., initial damage rates, are proportional by the Frenkel-pair resistivity (assumed to be 2×10^{-4} Ω cm for copper)[1] to the total cross sections for Frenkel-pair production. On the assumption that the bulk damage-rate curves (damage rate versus irradiation-induced electrical resistivity) for copper are linear,[21] initial damage rates were determined from the y intercept of the line defined by the size-effect-corrected damage rate and the saturation resistivity, which was experimentally determined in an 1100-keV irradiation by linear extrapolation (see Fig. 3) to be 522 $n\Omega$ cm.

The experimentally obtained total cross sections for Frenkel-pair production, $\sigma_d(\Theta_1,\Phi_1;E_1)$, are plotted in Fig. 4 as a function of the direction of the incident electron beam (Θ_1,Φ_1) for several different electron-beam energies, E_1. The unit triangle in the upper left of each panel shows the exact beam directions plotted in that panel. The error in the beam direction was ~1°; the largest contribution to this error was from slight intrinsic bends of the specimen. Each plot represents one scan (a tilt path with approximately constant Φ_1) across the unit triangle. The scans shown in Fig. 4(a), (c), and (d) are from a single specimen. Comparison with Fig. 4(b), taken from a different specimen, shows the reproducibility of the results from specimen to specimen. As expected, there were only minor differences in the total cross sections for Frenkel-pair production at small values of Θ_1 because these data were concentrated in a narrow angular region around the ⟨100⟩ direction. With increasing Θ_1 and Φ_1, differences ap-

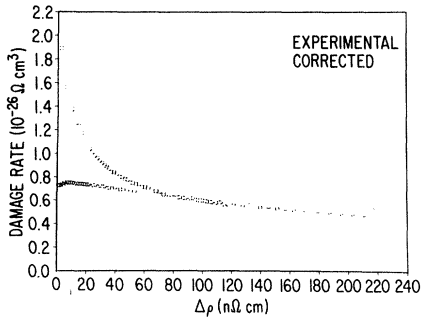

FIG. 3. Damage rate curves showing the experimental and size-effect corrected data for the ⟨100⟩ specimens used in the threshold anisotropy analysis irradiated at 1100 keV.

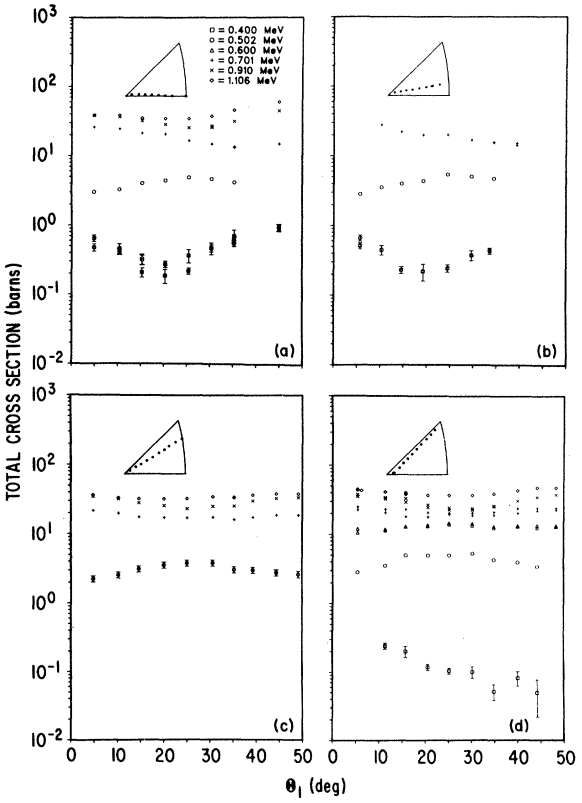

FIG. 4. Experimentally measured total cross section for Frenkel-pair production as a function of incident electron-beam direction and energy. Exact beam directions are shown in the insets.

peared in the measured total cross sections for Frenkel-pair production due to the anisotropy of the threshold energy. The detailed shape of these curves contained the necessary information to extract the threshold-energy surface. The size-effect correction was checked by measuring some total cross sections for Frenkel-pair production more than once. In general, the corresponding damage-rate measurements were carried out at different values of irradiation-induced electrical resistivity and thus required a different magnitude of size-effect correction. The agreement and reproducibility of these corrected damage rates indicated that the size-effect correction technique was adequate.

B. Analysis

The threshold-energy surface derived in the present study is shown in Fig. 5. Figure 5(a) gives

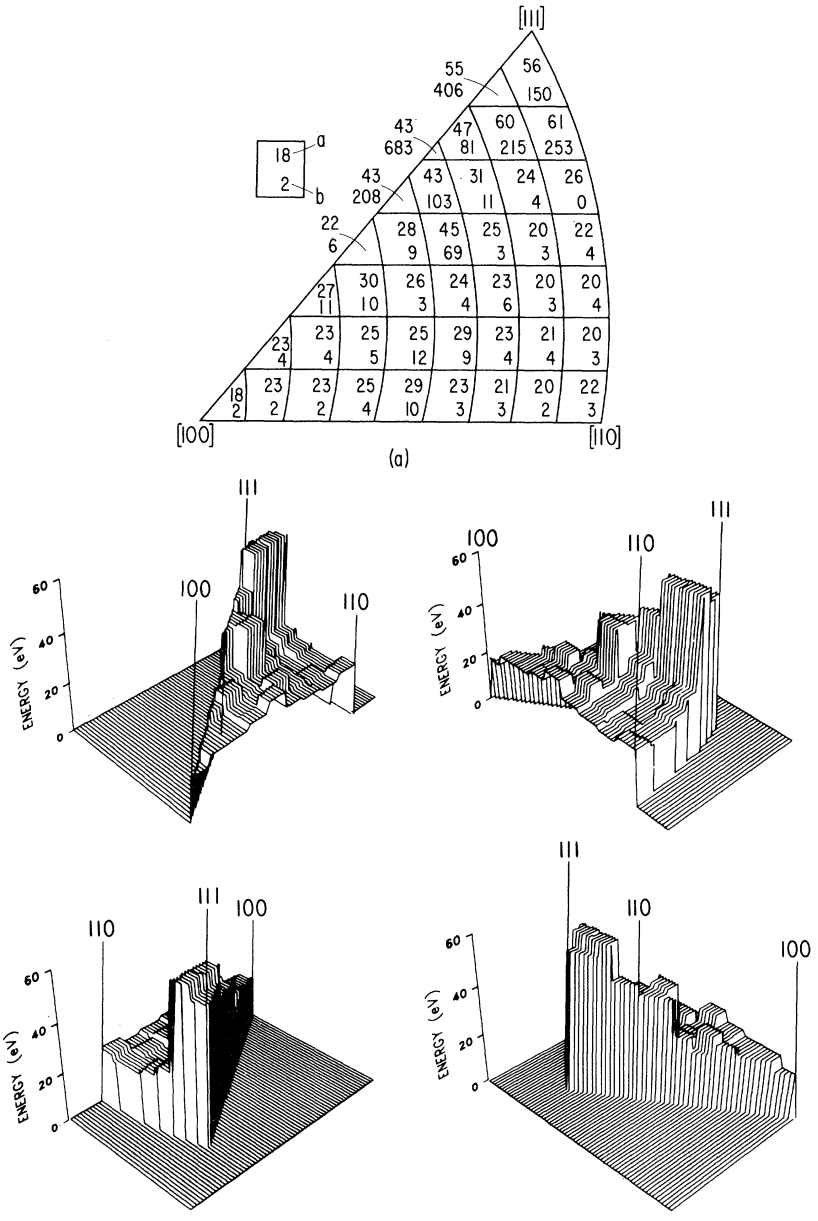

FIG. 5. The threshold-energy surface for copper, as derived in the present work. (a) Best-fit values, denoted by a, and sensitivity of fit, denoted by b, for each of the 41 (5°×5°) regions. (b) Four views of the contour plot.

the best-fit threshold-energy values, denoted by a, and the sensitivity of fit, denoted by b, for each of the 41 (5°×5°) regions. The sensitivities of fit give an estimate of how much the value of each threshold-energy region could vary such that χ^2 would not change by more than 10–25%. More specifically, if any threshold-energy region were increased in value by its respective sensitivity, χ^2 could be expected to increase by ~10%. On the other hand, if any region were decreased in value by its respective sensitivity, χ^2 could be expected to increase by ~25%. (This is because we are primarily sensitive to the lower threshold-energy regions.) Since the fitting procedure is sensitive to the local gradient of χ^2 for any particular threshold-energy region (i.e., $T_d \pm 1$ eV) and the sensitivities are unconstrained, very large values of the sensitivities are possible in the "insensitive" threshold-energy regions. For the case where the threshold energy would be decreased by the sensitivity (as mentioned above), physically unrealistic results are obtained (e.g., 56–150 eV near ⟨111⟩). A trial-and-error approach was taken to find the lower-limit threshold energy for the insensitive regions. This was determined to be ~30 eV (see error bars Fig. 6). The best-fit surface, plotted in Fig. 5(b), corresponds to the surface that gave the value of χ^2 closest to one. This is a contour plot of the unit triangle with the Z axis corresponding to the threshold energy. The average threshold energy for the best-fit threshold-energy surface is 28.5 eV; the minimum is 18 ± 2 eV and is located near ⟨100⟩. A ring of very high threshold energy (>50 eV) surrounds the ⟨111⟩ direction. The damage function derived from this surface is shown in Fig. 6. The error bars indicate the sensitivities of fit described above. The error bars at high recoil energy were truncated at 30 eV since values below this cause significant increases in χ^2. The function rises rather sharply from a value of zero at 17 eV to 0.8 at 42 eV. It has a value of 0.5 at 24.5 eV. Above 30 eV the slope of the curve begins to decrease, reflecting the presence of high-energy regions of the threshold-energy surface. In Sec. VII, this damage function will be applied to defect-production calculations for ion irradiations.

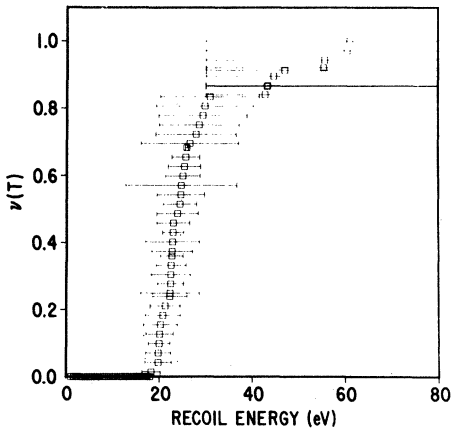

FIG. 6. The damage function for $\nu(T) < 1$ derived from the best-fit threshold-energy surface of Fig. 5. The error bars indicate the values for the sensitivity of fit.

VI. DISCUSSION

A. Topographical comparisons

Although a number of investigations have been carried out to study particular aspects of the threshold-energy surface in copper, we restrict our discussion to those investigations that resulted in a detailed threshold-energy surface. A summary of the investigations on copper is given in Table III of the Appendix.

Gibson *et al.*,[22] using a dynamic computer code with a Born-Mayer potential, calculated the threshold-energy surface for copper shown in Fig. 7(a). The threshold-energy surface has been interpolated and divided into 41 (5°×5°) blocks to facilitate comparison with the threshold-energy surface derived in the present work. The minimum threshold energy in ⟨100⟩ was found to be the same or slightly lower than the threshold energy in ⟨110⟩; these values are 25 eV and 25–30 eV, respectively. The threshold energy for ⟨111⟩ was substantially higher, ~85 eV. The surface varied quite smoothly from ⟨100⟩ and ⟨110⟩ to ⟨111⟩. The average threshold energy for this surface was 44 eV.

Schwartz *et al.*,[10] using the quasidynamic computer code ADDES with the Moliére approximation to the Thomas-Fermi screening function to describe the pair interactions, determined threshold energies for 20 directions distributed over the unit triangle. These results are shown in Fig. 7(b), again interpolated and divided into 41 (5°×5°) blocks. Each of the major directions, ⟨100⟩, ⟨110⟩, and ⟨111⟩, is a local minimum in the threshold energy. The average threshold energy for this surface is 43 eV.

Jung *et al.*[9] irradiated single-crystal copper specimens with electrons in enough directions to acquire electrical-resistivity data from the perimeter of the unit triangle. The threshold-energy surface was deduced from a computer fit to ~40 normalized damage rates measured for five energies between 1.13 and 1.89 MeV using ~40 adjustable parameters; Figs. 7(c) and 7(d) show limits of the range of values given by the authors. The minimum threshold energy resides away from

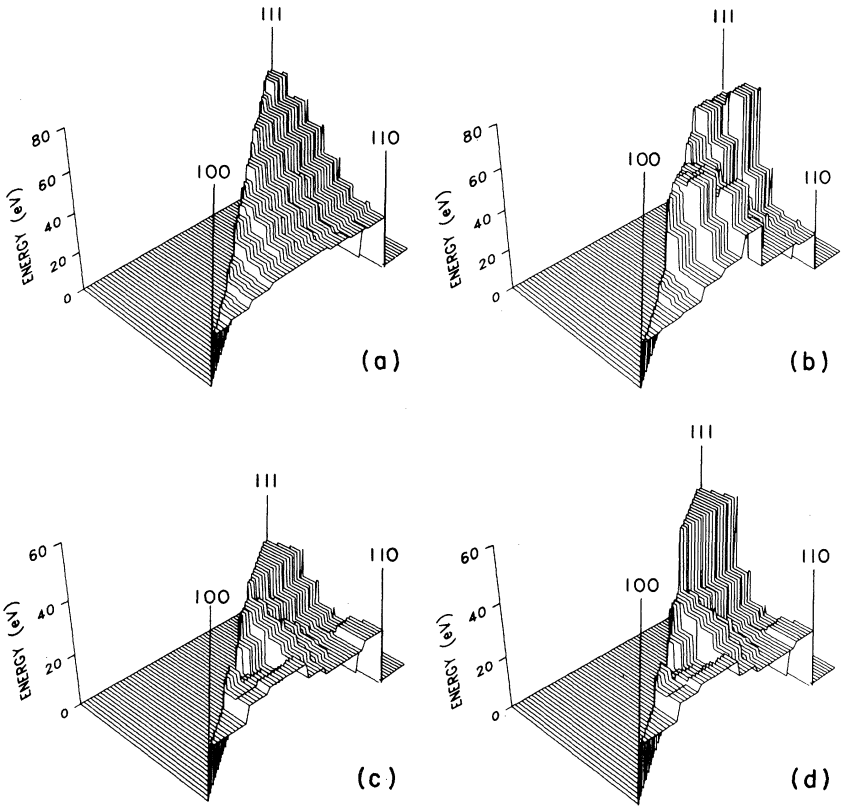

FIG. 7. Contour plots showing the threshold-energy surfaces derived for copper by (a) Gibson *et al.* (Ref. 22), (b) Schwartz *et al.* (Ref. 10), and (c) and (d) Jung *et al.* (Ref. 9).

the ⟨100⟩ and ⟨110⟩ directions with values of 19–22 eV. The average threshold energy deduced from this surface was 26–30 eV.

Remarkable similarities are found when comparing the main features of the topography of the four threshold surfaces considered here. In all cases, the minimum threshold regions are found near the two most closely packed directions. For any given surface, the magnitude of the threshold energies along ⟨110⟩ and ⟨100⟩ are very similar. Considerable structure is indicated by all surfaces except the one derived from the computer calculations of Gibson *et al.* This is due to the relatively small number of directions that were investigated. A further similarity of the surfaces of Schwartz *et al.*,[10] Jung *et al.*,[9] and the present one is the size of the low threshold-energy region around ⟨110⟩, which extends to about 15° from this pole. This clearly seems to be a reflection of the ease of separating interstitials from vacancies via replacement collision sequences. The question whether there is local minimum in the exact ⟨110⟩ and ⟨100⟩ directions as found in the computer calculations, can not be answered unambiguously from the present work. Although the present results suggest that there are low threshold energies in both of these directions, it is also evident from the present work that the same or even lower threshold energies can be obtained in directions ~10° to 15° off the two major close-packed directions. The relatively large differences between some adjacent 5°×5° blocks in this surface indicate that more fine structure is present than was possible to resolve in the present work. The finite resolution that had to be used in the present work to describe the threshold-energy surface is largely due to the number of data points and their angular separation; however, it would be possible and desirable to explore the regions around ⟨110⟩ and ⟨110⟩ with somewhat higher resolution. Particularly, the question of whether extremely narrow angular regions of very low threshold energy[23] are present, would be of interest for our understanding of basic displacement mechanisms.

B. Quantitative comparisons

One might ask whether the differences among these threshold-energy surfaces are significant. Unfortunately, topographic features alone do not indicate the capability of the threshold-energy surface to predict defect production, which is one

of the primary reasons for deriving it. In order to quantitatively compare the threshold-energy surface derived in the present work with those of Refs. 9, 10, and 22, the total cross sections for Frenkel-pair production were calculated from each of these surfaces and the results were compared with the total cross sections measured in the present work. The χ^2 statistics calculated for the four threshold-energy surfaces are given in Table I. A comparison of these statistics indicates that the present threshold-energy surface predicts the total cross sections for Frenkel-pair production considerably better than the others.

In order to make a more detailed comparison between the threshold-energy surfaces and our experimental data, the calculated and measured total cross sections for Frenkel-pair production were plotted in Fig. 8 as a function of incident-beam direction and energy. (The exact irradiation directions are shown in the unit triangles in the upper left of each panel.) The curves represent the cross sections calculated from the threshold-energy surfaces given in the present work and in Refs. 9, 10, and 22. The shaded area represents the range of cross sections predicted by the surface of Jung *et al.*[9] The experimental data from the present work are plotted with error bars which include a 10% uncertainty in the Frenkel-pair resistivity. The following general comments can be made about Fig. 8. (1) The threshold-energy surface of Gibson *et al.*[22] consistently underestimates the total cross sections for Frenkel-pair production that were observed experimentally, and the cross-section curves usually differ markedly in shape from the experimental curves. (2) The surface of Schwartz *et al.*[10] also underestimates the total cross sections for Frenkel-pair production that were observed experimentally; however, the shapes of the cross-section curves usually conform closely to the shapes of the experimental curves. A linear scaling of this surface, which was carried out to improve the fit to the experimental curves, not only changed the absolute magnitude of the total cross sections for Frenkel-pair production, but also significantly changed the shape of the cross-section curves. This means that both the magnitude and topography of the surface are inconsistent with our data. (3) The measured total cross sections for Frenkel-pair production generally fell within the range calculated from the surface of Jung *et al.*,[9] which suggests that the best-fit surface would have values somewhere within the range of threshold-energy values given by these authors. (4) In 4 cases [Fig. 8(e), (h), (j), (p)], the lower-limit surface of Jung *et al.*[9] gave the best fit to the experimental data; in 1 other case [Fig. 8(o)] the upper-limit surface of Jung *et al.*[9] gave the best fit. In the remaining 11 cases, the threshold-energy surface of the present work gave the best fit to the data. Table II gives the value of χ^2 for each plot in Fig. 8. The variation in χ^2 from plot to plot for our surface is quite small compared to the other surfaces. It should be noted that the work of Jung *et al.* would be expected to give consistently lower χ^2 values in Table II for any surface in between the lower- and higher-limit surfaces.

TABLE I. χ^2 statistics comparing total cross sections for Frenkel-pair production, as calculated from various threshold-energy surfaces, with total cross sections measured in the present work.

Threshold-energy surface from	χ^2
Present work	1.45
Jung *et al.*[a]	better than 7.90–8.72[d]
Schwartz *et al.*[b]	37.8
Gibson *et al.*[c]	81.2

[a] Reference 9.
[b] Reference 10.
[c] Reference 22.
[d] Jung *et al.* give a range of values for the threshold-energy surface. The χ^2 values refer to the two extreme surfaces.

C. Special considerations

We emphasize that the present analysis was carried out using the commonly accepted value of $\rho_F(2\times10^{-4}\ \Omega\ \text{cm})$. Evidence exists that ρ_F may also be treated as a free parameter; however, this is beyond the scope of the present work and will be covered in a separate presentation.

This analysis has been based upon the critical assumption given in Eq. (3). In contradiction to this assumption, the computer-simulation studies of Schiffgens and Bourquin[24] show that for certain energies and directions, $\nu(\Theta_2,\Phi_2;T)=0$ for $T>T_d(\Theta_2,\Phi_2)$. It has been suggested[25] that this "nonmonotonic" behavior of ν may invalidate the analyses of single-crystal data. Recently, King and Benedek[26] have carried out detailed computer simulations to investigate the pervasiveness of the nonmonotonic behavior. It was found that the nonmonotonic behavior is restricted to directions where the defect-production mechanism is considerably more complex than a simple replacement collision chain along a low-index direction. These correspond to high-threshold-energy directions where electron-irradiation damage-rate experiments are relatively insensitive. On the other hand Eq. (3) was found to be well satisfied for the directions that dominated the defect-production process. Thus, the breakdown of Eq. (3) in the high-threshold-energy directions is not expected to strongly

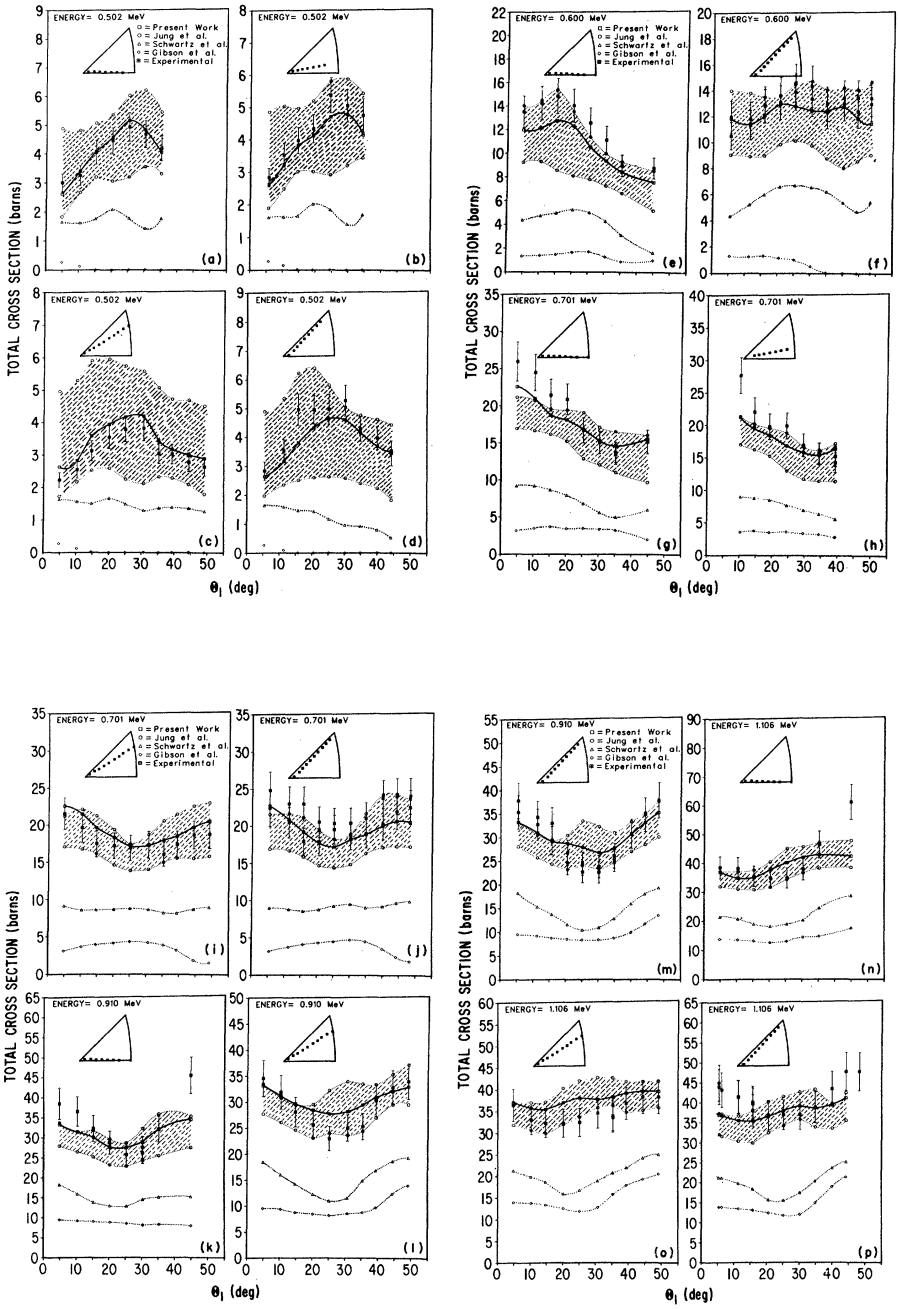

FIG. 8. Measured total cross sections for Frenkel-pair production in copper (present work), compared with the total cross sections calculated from threshold-energy surfaces derived in the present work, and reported previously for the beam directions shown in the upper left.

influence the general features of the experimental threshold-energy surface.

One might ask if our results were biased by our "first-guess" threshold-energy surface. To check this we chose another first-guess surface in which each of the 41 regions had the value 24 eV. After carrying out the 41-parameter minimization, the resulting surface was only slightly worse in fit than than our best-fit surface ($\chi^2 = 1.68$). In the 33 regions with good sensitivity of fit, 30 had values that matched the corresponding regions in the best-fit surface within the error specified by the sensitivity of fit for that region. Thus we conclude that the fitting technique was only slightly

TABLE II. χ^2 statistics for the curves in Fig. 8 illustrating the goodness of fit to the corresponding experimental data.

Panel of Fig. 8	Present work	Curve derived from Jung *et al.*[a] Lower-limit surface	Higher-limit surface	Schwartz *et al.*[b]	Gibson *et al.*[c]
a	0.32	13.3	7.66	31.6	92.9
b	0.69	11.7	10.6	33.9	92.5
c	1.22	58.3	7.85	26.3	94.0
d	1.11	10.2	17.6	46.8	86.6
e	1.77	0.31	13.3	43.8	77.7
f	0.61	1.53	8.50	30.0	86.4
g	0.91	2.23	7.05	37.7	65.6
h	1.39	1.30	7.89	35.6	63.7
i	0.58	3.04	2.26	26.7	64.4
j	1.02	0.82	8.86	31.3	65.9
k	1.33	2.14	5.17	28.9	52.6
l	1.03	4.37	1.42	22.7	44.0
m	1.27	5.17	2.53	27.4	46.1
n	1.88	2.58	3.25	22.3	42.3
o	1.08	3.80	0.49	17.3	31.2
p	1.28	1.24	4.89	26.3	41.5

[a] Reference 9.
[b] Reference 10.
[c] Reference 22.

biased by the first guess, away from some local minima in the neighborhood of the best fit.

It is important to note that the interstitial population created during irradiation is made up of a distribution of Frenkel-pair configurations and that the relative population of these configurations depends critically upon the corresponding distribution of recoil directions and recoil energies. The possibility exists that some of these configurations may become unstable under the influence of thermal spike effects due to nearby electron-atom collisions. This effect could cause diminution of the observed total cross section for Frenkel-pair production or subthreshold annealing if it occurred with great frequency, and may depend on defect concentration, irradiation energy, and irradiation direction. Although for each angular scan, the total resistivity increase (above the residual resistivity) was kept as small as possible, usually <30 $n\Omega$cm to minimize the effect of subthreshold annealing, a test was carried out as suggested by Andersen and Sørensen,[27] to determine if the effect of subthreshold annealing on the present data was negligible. The influence of subthreshold annealing on this experiment was checked by (1) carrying out the anisotropy experiment by superimposing the Frenkel pairs created during test irradiations on different concentrations and configurations of Frenkel pairs, and (2) reprobing some intermediate irradiation directions following a complete angular scan.

The anisotropy experiment was carried out, beginning with an undamaged specimen, at 600, 701, and 910 keV with a total increase in the sample resistivity of ~ 90 $n\Omega$cm. In these experiments, Frenkel pairs created during the higher-energy test irradiations were superimposed on those created at lower energies. The samples were then annealed to room temperature and experiments were again carried out at 910, 701, and 600 keV (reverse order). Between each energy, the samples were annealed above stage I. Comparison of the results of these two experiments [given in Figs. 4(d), 8(f), 8(j), and 8(m)] indicate that any subthreshold annealing that resulted from the superposition of test irradiations on different configurations and concentrations of Frenkel pairs did not influence the experimental results.

At 1100 and 700 keV, experiments were carried out where the standard tilting procedure was followed. After this was completed, some intermediate irradiation directions were sampled again. These results are shown in Fig. 4(a), (b), and (d) and Fig 8(g), (e), and (p) and indicate that subthreshold annealing did not depend in any significant way on the tilting procedure.

D. Comparisons with the experiment of Jung *et al.* (Ref. 9)

It comes as no surprise that the threshold-energy surface as derived in the present work predicts the measured total cross sections for Frenkel-pair production better than the other available surfaces, since that is the purpose of the optimization scheme. The burden of proof for the acceptance of these results clearly falls upon the reliability of our experimental results. At this point, it is appropriate to compare our experimental technique to those of typical accelerator experiments, for example, the technique of Jung *et al.*[9] The magnitude of the variation or anisotropy of the damage rate or total cross section with crystal direction that was measured by our technique (Fig. 4) was a factor of ~3 greater than that observed by Jung *et al.*[9] The reason for this is twofold. First, we expect the effects of the threshold anisotropy to be most pronounced at energies near to the threshold energy as in our case and second, many of the experimental complications that were present in typical accelerator experiments that may have reduced the observed anisotropy of the damage rate were less important in our experiment. The following complications were present in the work of Jung *et al.*: (1) The electron-beam divergence before hitting the specimen was significant, (2) the electron beam was substantially broadened by multiple scattering within the specimens, (3) the specimen alignment with respect to the electron beam and the specimen flatness were difficult to determine accurately, (4) multiple displacements may have been possible at the energies used, (5) and the number of degrees of freedom in the fitting procedure was nearly zero.

The anisotropy of the damage rate may be reduced if the electron beam is nonparallel before entering the specimen. Jung *et al.* used a bath-type cryostat in their experiment, where the beam had to penetrate a 1-μm stainless-steel window and pass through a layer of liquid helium before reaching the specimen.[28] This may cause the beam to diverge as much as ~10°.[29] This violates our assumption of an initially parallel beam and must be factored into Eq. (4) as a distribution of incident electron-beam directions. In our case, however, there is no physical obstruction of the beam before it encounters the specimen and the electron optics are such that the beam divergence was 0.04°.

The distribution of incident-beam directions becomes broader as the electrons traverse the material. Multiple scattering, which increases with the specimen thickness, causes a reduction in the observed anisotropy of the damage rate and a slight increase in the observed damage rate. In the experiment of Jung *et al.*,[9] specimens were on the order of 15 μm thick where multiple scattering caused the electrons to scatter in nearly every crystal direction.[6] In our experiments the specimens were ~0.4 μm thick. In this thickness regime and the energy range 0.5–1.1 MeV, multiple scattering is expected to be smaller than that in the experiment of Jung *et al.*[6]

A very important factor in these threshold anisotropy experiments is the ability to accurately align the specimen with respect to the incident-beam direction. Because the reduction in the observed anisotropy due to multiple scattering is more severe than slight misorientations of the sample, accurate specimen alignment was not so critical in the experiment of Jung *et al.* In our experiments, the specimens were oriented using Kikuchi patterns and maps to ensure that the beam directions were accurately determined to within 1°.

In order to assure that the assumption that only single defects are formed during an irradiation is not violated, the energies used in the anisotropy experiment should be chosen such that the probability of multiple-defect production is small. Schiffgens and Bourquin's computer results[24] show that the onset for multiple-defect production in copper occurs at recoil energies between 75 and 100 eV, corresponding to beam energies greater than 1.1 MeV. Jung *et al.* used energies from 1.13 to 1.89 MeV in their analysis, corresponding to maximum transferred energies of ~82 to 186 eV. Our experiments were carried out in the energy regime where one expects only single-defect production, 0.5 to 1.1 MeV, corresponding to maximum transferred energies of ~19 to ~80 eV. This is shown more clearly by considering the values of the median recoil energies ($T_{1/2}$, recoil energy below which $\frac{1}{2}$ of the defects are produced); 23.7, 26.3, 28.3, 31.8, and 34.7 eV for irradiation energies of 0.502, 0.600, 0.701, 0.910, and 1.106 MeV, respectively. To avoid including the effects of subthreshold defect production, we deleted the 0.4-MeV data from the analysis. From other experiments that we carried out on similar copper specimens, we estimate the contribution due to subthreshold defect production to be ~0.5 barns.

In their efforts to find the best-fit threshold-energy surface consistent with their data, Jung *et al.*[9] selected 40 damage-rate values from around the perimeter of the unit triangle. The number of adjustable parameters in their calculation was about 40 so that the number of degrees of freedom in their fitting procedure was nearly zero. In our case, to promote reliability of our best-fit thresh-

old-energy surface, the number of degrees of freedom was ~120. It is interesting to note, that in spite of these substantial difficulties associated with conventional accelerator experiments, our observed total cross sections for Frenkel-pair production as well as the total cross sections derived from our surface fall, in most instances (see Fig. 8), well within the limits given by the total cross sections derived from the surfaces of Jung *et al.* when our analysis is based on $\rho_F = 2.0 \times 10^{-4}$ Ω cm. However, we should emphasize that the significant reduction in experimental complications that was realized using our experimental technique provided the basis for a more clear, unambiguous picture of the threshold-energy surface than has been possible in the past.

A quantitative comparison, as in Sec. VI B, was also carried out using the damage-rate data of Jung *et al.* and the surfaces of that work and the present work. Since corrections to measure damage rates for multiple scattering are quite difficult, we made no attempt to correct Jung *et al.*'s measured damage rates for multiple scattering. A value for the Frenkel-pair resistivity of 2.0×10^{-4} Ω cm (as opposed to 1.7×10^{-4} Ω cm) (Ref. 9) was used to obtain total cross sections for Frenkel-pair production. We expected that due to multiple scattering, the data of Jung *et al.* would exhibit less anisotropy than the calculated total cross sections for Frenkel-pair production and that the magnitude of the measured total cross sections for Frenkel-pair production would be, due to the increased path length, slightly higher than the calculated total cross sections for Frenkel-pair production. The observed anisotropy was clearly smaller than the calculations predicted. As expected when using a larger ρ_F value, the magnitude was in general at or below the lower end of the range of cross sections predicted by the threshold-energy surface of Jung *et al.* It was found that the upper limit of Jung *et al.*'s threshold-energy surface [Fig. 7(d)] fit their data quite well ($\chi^2 = 1.27$). Clearly, the surface of Jung *et al.* would have been somewhat different if a value of $\rho_F = 2.0\times10^{-4}$ Ω cm would have been used. However, the bounds in the surface as derived by Jung *et al.* are fully consistent with our present threshold-energy surface based on $\rho_F = 2.0\times10^{-4}$ Ω cm.

VII. APPLICATION TO DEFECT PRODUCTION AT HIGHER ENERGIES

For many calculations of defect production at higher energies, the Kinchin and Pease[30] or modified Kinchin and Pease[31] models for the damage function are often used. The modified Kinchin and Pease damage function uses a sharp threshold and has the form

$$\nu(T) = \begin{cases} 0 \text{ for } T < \langle T_d \rangle; \\ 1 \text{ for } \langle T_d \rangle \leq T \leq 2.5\langle T_d \rangle; \\ \dfrac{0.8\epsilon(T)}{2\langle T_d \rangle} \text{ for } 2.5\langle T_d \rangle < T, \end{cases} \tag{7}$$

where $\langle T_d \rangle$ is the average threshold energy and $\epsilon(T)$ is the damage energy associated with a target atom of recoil energy T.[31] The inadequacy of this simple damage function for defect-production calculations at high recoil energies is shown in Fig. 9 in which the damage efficiency ξ [the ratio of the observed total-displacement cross section to a calculated total-displacement cross section based on Eq. (7)], is plotted as a function of the median recoil energy $T_{1/2}$. Deviation of ξ from unity reflects the differences between the model and the physical case. Averback, Benedek, and Merkle[30] have shown via extensive ion irradiation studies that the damage efficiency ξ, based on the modified Kinchin and Pease expression [Eq. (7)], decreases drastically at high recoil energies. In the following, the effect of different threshold surfaces and thus the effect of the detailed shape of the damage function at $\nu(T) \leq 1$ on damage calculations shall be examined. The damage function that was derived in the present work, as well as those derived from the other threshold-energy surfaces, was substituted for the step function in the modified Kinchin and Pease model and the average

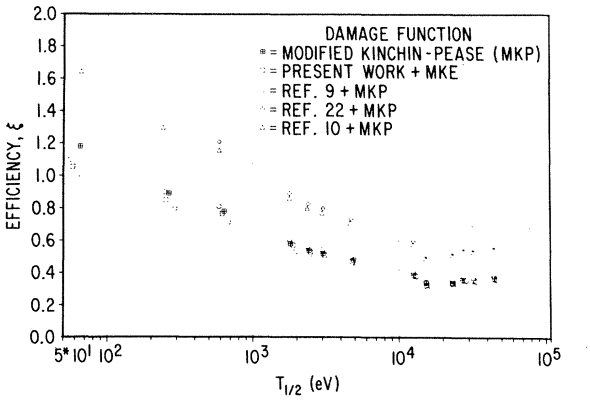

FIG. 9. The damage efficiency for ion irradiation of copper as a function of the median recoil energy $T_{1/2}$, based on the experimental work of Averback, Benedek, and Merkle (Ref. 31) and six different damage functions.

TABLE III. Summary of work performed to determine the anisotropy of the threshold energy in copper.

Metal	Orientation	Threshold energy (eV)	Technique	Comments	Specimen thickness (μm)	Energy range (MeV) Low	High	Authors	Ref.
Cu	⟨100⟩	19	Resistivity	b,d	10			Sosin and Garr (1965)	32
	⟨110	19	Resistivity	b,d	6.8				
	~⟨110⟩	28–30	Resistivity	f,d	35	0.4	1.0	Kamada *et al.* (1964)	33
	~⟨110⟩	9	Resistivity					Wollenberger and Wurm (1965)	34
								Bauer and Sosin (1964)	35
	⟨100⟩	>30	HVEM	b,c	0.5	N/A	N/A	Makin (1968)	36
	⟨110⟩	>30	HVEM	b,c	0.5	N/A	N/A		
	⟨100⟩	21.6	HVEM	b,c	<1	N/A	N/A	Makin (1970)	37
	⟨110⟩	19.2	HVEM	b,c	<1	N/A	N/A		
	⟨111⟩	23.6	HVEM	b,c	<1	N/A	N/A		
	⟨100⟩	20–22	Resistivity	a,d	15	1.0	2.0	Jung *et al.* (1973)	9
	⟨110⟩	22–23	Resistivity	a,d	15	1.0	2.0		
	⟨111⟩	40–50	Resistivity	a,d	15	1.0	2.0		
	⟨100⟩	15.18/27.5	HVEM	b,c	0.4	0.250	0.650	Kenik and Mitchell (1975)	38
	⟨110⟩	18	HVEM	b,c	0.4	0.250	0.650		
	⟨111⟩	19.2/ 29.2	HVEM	b,c	0.4	0.250	0.650		
	~⟨110⟩	9.5	HVEM	b,c	0.3	0.220	0.400	Yoshida and Urban (1977)	23
	⟨100⟩	22	Computer	N/A	N/A	N/A	N/A	Schwartz *et al.* (1976)	10
	⟨110⟩	20	Computer	N/A	N/A	N/A	N/A		
	⟨111⟩	63	Computer	N/A	N/A	N/A	N/A		
	⟨100⟩	25	Computer	N/A	N/A	N/A	N/A	Tenenbaum (1978)	39
	⟨110⟩	25	Computer	N/A	N/A	N/A	N/A		
	⟨100⟩	25	Computer	N/A	N/A	N/A	N/A	Gibson *et al.* (1960)	22
	⟨110⟩	25–30	Computer	N/A	N/A	N/A	N/A		
	⟨111⟩	~85	Computer	N/A	N/A	N/A	N/A		
	⟨100⟩	8.5–15	Dislocation pinning	N/A	19	0.25	2.8	Roth *et al.* (1975)	40
	?	17–22	Dislocation pinning	N/A	?	0.35	2	Lauzier *et al.* (1979)	41

[a] Computer fit—many adjustable parameters.
[b] Apparent threshold energy.
[c] Room temperature or above.
[d] Helium temperature.
[e] Computer fit—few adjustable parameters.
[f] Apparent threshold energy—subthreshold effects factored out.
[g] N/A=not applicable.

threshold energy as determined for each surface was substituted for $\langle T_d \rangle$. In this manner, and by using an otherwise identical defect production model as in Ref. 31, modified efficiency values were obtained. These are shown in Fig. 9 together with the values based on a sharp threshold.[31]

In agreement with the comparisons in Sec. VI, the surfaces derived by Gibson *et al.*[22] and Schwartz *et al.*[10] underestimate the defect production. This is mainly a result of the rather high average threshold energies obtained in the dynamical simulations and implies that improved interatomic potentials are needed to get closer agreement with experiment.

The effect of the detailed shape of the damage function at $\nu(T) \leq 1$ on damage calculations is seen when the damage function from the present investigation is compared with the modified Kinchin and Pease damage function, because both functions are identical for $\nu(T) > 1 (\langle T_d \rangle = 28$ eV). At effective median recoil energies $T_{1/2} < 100$ eV, as obtained in proton bombardments, the detailed shape of the damage function for $\nu(T) < 1$ obviously has a significant effect on the total defect production (~15%). Both the surfaces of Jung *et al.* as well as the surface derived in the present work give a significant improvement over the sharp threshold approximation. At low recoil energies ion-damage predictions are now in rather close agreement with the observations. As expected the differences between calculations based on a sharp threshold and the detailed damage function for $\nu(T) < 1$ become insignificant in the 1

to 100 keV region, where primarily displacement cascades are produced. It should be pointed out that one of the great merits of a detailed determination of the threshold anisotropy is to provide a value for the average threshold energy which can be used as a basis for quantitative comparisons of damage production at high recoil energies. As before, the present results fall between those of Jung *et al.*[9] Within the experimental error of the measured total cross sections from the ion irradiations, no one of these damage functions can be singled out as the best.

The fact that the efficiency deviates widely from unity for higher $T_{1/2}$ indicates that the damage function at high energies is not well described by the simple cascade theories.[31] Several indications exist that cascade dynamics play a significant role in the resultant defect structure, but discussion of this is beyond the scope of this work.

VIII. SUMMARY

In situ damage-rate measurements on thin single-crystal copper films were carried out in the high-voltage electron microscope for electron irradiations in ~40 crystallographic directions at six energies from 0.4 to 1.1 MeV. Kikuchi patterns were used to align the specimens precisely. These experimental measurements were used to derive a threshold-energy surface for Frenkel-pair production. The average threshold energy of this surface is 28.5 eV. The minimum threshold energy is 18 ± 2 eV and is located near ⟨100⟩. A ring of very high threshold energy (>50 eV) surrounds the ⟨111⟩ pole. A damage function was derived from this surface and was applied to defect-production calculations at higher recoil energies. The present surface was compared both topographically and quantitatively with those in the literature. Based on a χ^2 goodness-of-fit test, the present surface was found to predict the experimentally observed total cross sections for Frenkel-pair production considerably better than the other available surfaces. Also, the goodness of fit varied substantially less with energy and direction for the present surface.

ACKNOWLEDGMENTS

The authors gratefully acknowledge the technical support of the Argonne National Laboratory High Voltage Electron Microscope-Tandem Facility and crew, the assistance of Dr. I. Hashimoto, and the valuable suggestions of Dr. R. Benedek who critically read this manuscript. Thanks are also due to Dr. O. S. Oen for calculating the ratio of Mott-to-Rutherford scattering in our energy regime, and to Mr. J. J. Kaganove for implementing the derivative-type optimization technique.

This work was supported by the National Science Foundation and the U. S. Department of Energy. Support by a Walter P. Murphy Fellowship from Northwestern University and a Laboratory Graduate Participantship from the Argonne Center for Educational Affairs for Wayne E. King, are gratefully acknowledged.

APPENDIX

Table III gives a summary of past threshold anisotropy studies in copper for the principal crystallographic directions. Specimen thicknesses and irradiation energies are shown and, in addition, threshold energies where applicable. Comments on the nature of each investigation are also given.

[1] P. Lucasson, in *Proceedings of the International Conference on Fundamental Aspects of Radiation Damage in Metals*, edited by Mark T. Robinson and F. W. Young, Jr. (National Technical Information Service, U. S. Dept. of Commerce, Springfield, Virginia, 1975), p. 42.

[2] P. Jung, in *Atomic Collisions in Solids*, edited by S. Datz, B. R. Appleton, and C. D. Moak (Plenum, New York, 1975), Vol. I, p. 87.

[3] K. L. Merkle, in *Radiation Damage in Metals*, edited by N. L. Peterson and S. D. Harkness (American Society for Metals, Metals Park, Ohio, 1975), p. 58.

[4] P. Vajda, Rev. Mod. Phys. 49, 481 (1977).

[5] Jorge J. Moré, in *Lecture Notes in Mathematics* (Springer, Berlin, 1978), pp. 105–116.

[6] M. Wilkens, in *Proceedings of the Fifth International Conference on High Voltage Electron Microscopy, Kyoto, Japan*, edited by T. Imura and H. Hashimoto (Japanese Society of Electron Microscopy, Tokyo, 1977), p. 475.

[7] O. S. Oen (private communication) and in *Cross Sections for Atomic Displacement in Solids by Fast Electrons*, Oak Ridge National Laboratory Report No. 4897, 1973.

[8] W. Bauer, A. I. Anderman, and A. Sosin, Phys. Rev. 185, 870 (1969).

[9] P. Jung, R. L. Chaplin, H. J. Fenzl, K. Reichelt, and P. Wombacher, Phys. Rev. B 8, 553 (1973).

[10] D. M. Schwartz, R. G. Ariyasu, J. O. Schiffgens, D. G. Doran, and G. R. Odette, in *Proceedings of the 1976 International Conference on Computer Simulation for Materials Applications, Gaithersburg, Maryland,*

April 1976 (National Bureau of Standards, Washington, D. C., 1976), pp. 75–88.
[11]Chr. Lehmann, *Defects in Crystalline Solids* (North-Holland, Amsterdam, 1977), Vol. 10.
[12]L. C. R. Alfred, Phys. Rev. 152, 693 (1966).
[13]F. Dworschak, H. Wagner and P. Wombacher, Phys. Status Solidi B 52, 103 (1972).
[14]E. H. Sondheimer, Adv. Phys. 1, 1 (1952).
[15]L. E. Thomas, Radiat. Eff. 5, 183 (1970).
[16]K. A. Shoaib and R. L. Segall, Philos. Mag. 22, 1269 (1970).
[17]P. A. Doyle, Philos. Mag. 29, 537 (1974).
[18]K. Izui, S. Furuno, H. Otso, T. Nishida, and H. Maeta, in *Proceedings of the Fifth International Conference on High Voltage Electron Microscopy, Kyoto, Japan,* edited by T. Imura and H. Hashimoto (Japanese Society of Electron Microscopy, Tokyo, 1977), p. 489.
[19]T. Nishida, K. Izui, and S. Furuno, Radiat. Eff. 34, 217 (1977).
[20]K. Urban and N. Yoshida, Radiat. Eff. 42, 1 (1979).
[21]G. Duesing, W. Sassin, W. Schilling, and H. Hemmerich, Cryst. Lattice Defects 1, 55 (1969).
[22]J. B. Gibson, A. N. Goland, M. Milgram, and G. H. Vineyard, Phys. Rev. 120, 1229 (1960).
[23]N. Yoshida and K. Urban, in *Proceedings of the Fifth International Conference on High Voltage Electron Microscopy, Kyoto, Japan,* edited by T. Imura and H. Hashimoto (Japanese Society of Electron Microscopy, Tokyo, 1977), p. 493; Phys. Lett. 63A, 381 (1977).
[24]J. O. Schiffgens and R. D. Bourguin, J. Nucl. Mater. 69 & 70, 790 (1978).
[25]P. Jung, Phys. Rev. B 23, 664 (1981).
[26]Wayne E. King and R. Benedek, Phys Rev. B 23, 6335 (1981).
[27]H. H. Andersen and H. Sørensen, Radiat. Eff. 14, 49 (1972).
[28]P. Jung and W. Schilling, Phys. Rev. B 5, 2046 (1972).
[29]P. Jung, Kernforschungsanlage, Jülich Report No. Jul.-729 FF Jülich, Germany, unpublished.
[30]G. H. Kinchin and R. S. Pease, Rep. Prog. Phys. 18, 1 (1955).
[31]R. S. Averback, R. Benedek, and K. L. Merkele, Phys. Rev. B 18, 4156 (1978); and J. Nucl. Mater. 75, 162 (1978).
[32]A. Sosin and K. R. Garr, Phys. Status Solidi 8, 481 (1965).
[33]K. Kamada, Y. Kazumata, and S. Suda, Phys. Status Solidi 7, 231 (1964).
[34]H. Wollenberger and J. Wurm, Phys. Status Solidi 9, 601 (1965).
[35]W. Bauer and A. Sosin, J. Appl. Phys. 35, 703 (1964).
[36]M. J. Makin, Philos. Mag. 18, 637 (1968).
[37]M. J. Makin, *Atomic Collision Phenomena in Solids* (North-Holland, Amsterdam, 1970), p. 205.
[38]E. A. Kenik and T. E. Mitchell, Philos. Mag. 32, 815 (1975).
[39]A. Tenenbaum, Radiat. Eff. 39, 119 (1978).
[40]G. Roth, H. Wollenberger, Ch. Zeckau, and K. Lücke, Radiat. Eff. 26, 141 (1975).
[41]J. Lauzier, P. Girard, and C. Minier, in *Proceedings of the Conference in Internal Friction and Ultrasonic Attenuation in Solids, Manchester, England* edited by C. C. Smith (Pergamon, Oxford, 1980).